ACS OMEGA

Open Access

http://pubs.acs.org/journal/acsodf

Article

Thermoluminescence Studies of Proton-Irradiated Cr-, Mg-Codoped β-Ga_2O_3

Published as part of ACS Omega virtual special issue "Jaszowiec 2023".

Duarte Magalhães Esteves,* Ana Luísa Rodrigues, Maria Isabel Dias, Luís Cerqueira Alves, Zhitai Jia, Wenxiang Mu, Katharina Lorenz, and Marco Peres

Cite This: *ACS Omega* 2023, 8, 47874−47882

Read Online

ACCESS | Metrics & More | Article Recommendations | Supporting Information

ABSTRACT: Chromium-doped Ga_2O_3, with intense Cr^{3+}-related red-infrared light emission, is a promising semiconductor material for optical sensors. This work constitutes a comprehensive study of the thermoluminescence properties of Cr-, Mg-codoped β-Ga_2O_3 single crystals, both prior to and after proton irradiation. The thermoluminescence investigation includes a thorough analysis of measurements with different β^- irradiation doses used to populate the trap levels, with preheating steps to disentangle overlapping peaks (T_M-T_{STOP} and initial rise methods) and finally by computationally fitting to a theoretical expression. At least three traps with activation energies of 0.84, 1.0, and 1.1 eV were detected. By comparison with literature reports, they can be assigned to different defect complexes involving oxygen vacancies and/or common contaminants/dopants. Interestingly, the thermoluminescence signal is enhanced by the proton irradiation while the type of traps is maintained. Finally, the pristine glow curve was recovered on the irradiated samples after an annealing step at 923 K for 10 s. These results contribute to a better understanding of the defect levels in Cr-, Mg-codoped β-Ga_2O_3 and show that electrons released from these traps lead to Cr^{3+}-related light emission that can be exploited in dosimetry applications.

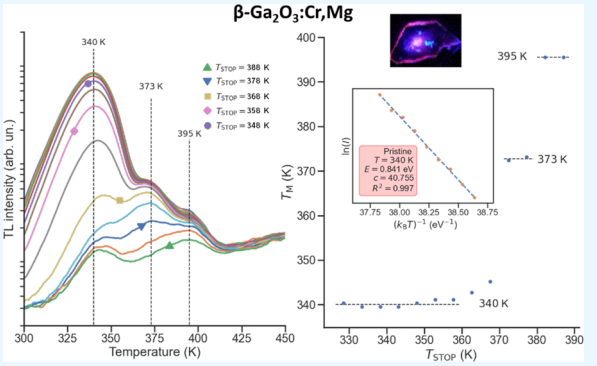

1. INTRODUCTION

Ga_2O_3 is a wide bandgap semiconductor that has recently attracted renewed attention of academia and industry alike due to its interesting properties. In particular, the high thermal and chemical stability of the monoclinic β phase, combined with its bandgap of ∼4.9 eV at room temperature (RT) and its large breakdown electric field of ∼8 MV/cm,[1−3] make β-Ga_2O_3 interesting for applications such as optoelectronic devices,[4] high-power electronics,[5] solar-blind ultraviolet (UV) photodetectors,[6] and gas sensors.[7] Moreover, due to its high transparency down to 260 nm,[1] β-Ga_2O_3 is an excellent host material for optically active centers emitting in the spectral region from the UV to the infrared (IR). In this context, Cr^{3+} is one of the most promising optically active ions in β-Ga_2O_3, with potential applications including ionizing radiation detection for active and passive optical dosimetry. In particular, the latter is especially promising in the context of in vivo dosimetry, given that the Cr^{3+} emission lies within the spectral region where biological tissue absorbs the least, known as the first biological window, spanning from 700 to 950 nm.[8]

For the previously mentioned reasons, there are several recent studies regarding the optical properties of Cr-doped β-Ga_2O_3. In particular, at RT, the characteristic luminescence associated with Cr^{3+} extends at least from 650 to 850 nm, comprising two sharp R-lines (namely, R_2 centered at ∼690 nm and R_1 at ∼697 nm) superimposed on a broad band with a maximum at ∼720 nm.[9,10] This emission has been previously explored in different applications, ranging from tunable optical microcavities[11] to luminescent thermometers[12] or radiation detectors.[13,14]

Despite the several potential applications associated with the incorporation of the Cr^{3+} ions into the Ga_2O_3 matrix, its complex excitation mechanisms are not fully understood yet. In fact, recent works suggest that the conditions under which the Cr^{3+} ions become optically active may be related with the sensitization of the emission by processes such as energy or charge transfer between defect levels in β-Ga_2O_3 and Cr^{3+} ions.[13−17] In this context, previous ion-beam-induced-luminescence (IBIL) measurements show a strong enhance-

Received: August 28, 2023
Revised: October 12, 2023
Accepted: October 17, 2023
Published: December 4, 2023

https://doi.org/10.1021/acsomega.3c06429
ACS Omega 2023, 8, 47874−47882

ment of the Cr^{3+} emission intensity as a function of the irradiation fluence as well as a reduction in electrical conductivity, thus suggesting that irradiation-induced defects play a major role in the activation of this luminescence.[13,14] These results are in line with several works showing a clear positive correlation between the Cr^{3+} luminescence yield and the electrical conductivity of the sample. Notably, semi-insulating samples have been found to exhibit higher luminescence yields compared to conductive ones.[13,14,18,19] It has been previously suggested that this dependence is related with different Cr^{2+}/Cr^{3+} concentrations due to different Fermi-level positions inside the bandgap.[18,19] While the Fermi-level position can be pinned lower in the bandgap by deep acceptors, such as Mg,[20] recent works comparing the Cr charge state in Mg-doped semi-insulating samples and conductive samples show that the charge state is 3+ in both cases.[13] Moreover, these works also show an enhancement in the Cr^{3+} luminescence yield with ion irradiation in the case of an electrically conductive sample.[13] It is, however, clear that the optical activation is intrinsically associated with the presence of defect levels that can sensitize the Cr^{3+} emission.[13,14,17,21]

Given its wide bandgap and its monoclinic lattice with several different inequivalent positions, the number of different possible defect states in β-Ga_2O_3 is quite high, as reported in several theoretical and/or experimental works resorting to techniques such as deep-level transient/optical spectroscopy (DLTS/DLOS) or thermoluminescence (TL).[14−16,21−27] Although it is notoriously difficult to unambiguously assign the observed levels with the corresponding defects, some of the experimentally measured trap levels have been attributed to intentional or unintentional dopants, such as Fe, Cr, and Mg, to intrinsic defects, such as O vacancies, or complex defects involving them (see Supporting Information). An energy level lying 0.7 eV below the conduction band has been reported and attributed to a complex involving Fe and intrinsic defects in multiple works.[21−23] Notably, a correlation between the density of these defects and the Cr^{3+} luminescence was observed.[15] Moreover, the charge transfer level Fe^{2+}/Fe^{3+}, lying 0.78 eV below the conduction band minimum,[23] has been proposed as a charge transfer channel to ionized Cr ions in the 4+ charge state.[21] Therefore, complexes involving Fe dopants (which is a common contaminant in Ga_2O_3[28]) are promising candidates to explain the activation of the elusive Cr^{3+} luminesce in β-Ga_2O_3.

In this context, this paper presents a detailed TL study performed on Cr-, Mg-codoped β-Ga_2O_3 on both pristine and 1−2 MeV proton-irradiated samples in order to assess both intrinsic and irradiation-induced defect levels in the optical activation and luminescence yield of the Cr ion.

2. RESULTS AND DISCUSSION

For this study, a single-crystal, Cr-, Mg-codoped β-Ga_2O_3 ribbon with a (100) surface orientation was grown by a modified edge-defined film-fed growth (EFG) method at the State Key Laboratory of Crystal Materials. Particle-induced X-ray emission (PIXE) and X-ray fluorescence (XRF) measurements confirmed the incorporation of Cr (0.028 atom %) and Mg (1.2 atom %) in the sample, as well as the presence of trace amounts of Fe (0.008 atom %), as previously reported (see Supporting Information).[13] Further details on the sample growth, IBIL, X-ray diffraction, and Raman spectroscopy results confirming its high crystalline quality can be found elsewhere.[13,14,28]

This crystal was cleaved into two different samples, one of which was kept pristine while the other one underwent proton irradiation using three different energies (1000, 1500, and 2000 keV), up to an irradiation fluence of 10^{15} protons/cm^2 for each energy (corresponding to 0.0029, 0.0024, and 0.0019 displacements per atom, respectively, as calculated at the vacancy profile maxima using Stopping and Ranges of Ions in Matter (SRIM) Monte Carlo simulations[29]). Under these conditions, SRIM simulations predict that the first ∼25 μm of the sample were damaged, with projected ion ranges of 8.74, 15.6, and 24.1 μm for each of the three ion energies, respectively, as shown in the Supporting Information. These irradiation conditions have been previously employed in similar samples.[14] Considering that the penetration depth of the electrons employed in this study is ∼500 μm, both the irradiated and the pristine regions are probed. Hence, by employing three energies, a large irradiated volume is achieved, which increases the TL signal coming from the implanted region and allows it to be discernible from the signal from the pristine region.

2.1. Preliminary TL Measurements. A preliminary TL measurement of the pristine and irradiated samples was performed, as shown in Figure 1, in order to assess whether the

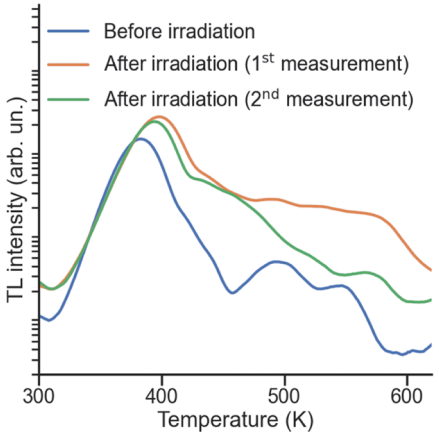

Figure 1. Preliminary TL glow curves for the pristine (before irradiation) and irradiated samples, in logarithmic scale. For the latter, two consecutive measurements are shown (1st and 2nd).

Cr ions were optically active before and after the irradiation. A typical TL measurement consists of two steps: an excitation step and a heating step. During the first, the sample is irradiated with ionizing radiation for a given time (β^- radiation for 400 s, in the present case, corresponding to a dose of 29.2 Gy in quartz coarse grains on stainless steel discs) in order to generate electron−hole pairs. Some of these electrons will then be trapped in defect levels. In the second step, the sample is heated with a constant heating rate up to a given temperature (up to 620 K, with a heating rate of 2 K/s, in the present case). The increased temperature promotes the release of the trapped electrons from the traps back to the conduction band. These released electrons then have a probability to recombine radiatively with holes at optically active centers, and the intensity of this emission is measured as a function of the temperature (in this case, this corresponds to the Cr^{3+} emission, which was monitored at ∼630 nm). Hence, apart

https://doi.org/10.1021/acsomega.3c06429
ACS Omega 2023, 8, 47874−47882

from assessing the presence of trap levels and their activation energy, this technique also provides valuable information regarding the complex trapping/detrapping probabilities via the so-called kinetics order parameter b: for $b = 1$, the probability of retrapping a thermally released electron is negligible, whereas for $b = 2$, the retrapping and radiative recombination probabilities are similar.[30]

These results show that the Cr^{3+} ions are optically active in the pristine sample, in agreement with photoluminescence (PL) and IBIL spectra obtained in previous works, but in contrast to samples without Mg-codoping that did not show significant Cr-luminescence in their pristine state.[13] This result is also consistent with a recent report observing the Cr^{3+} luminescence in electrically resistive Mg-codoped samples, in contrast with conductive Cr-doped β-Ga_2O_3 samples, which displayed lower Cr^{3+} luminescence yields.[18] This difference was attributed to the different Fermi-level locations: in the case of the conductive samples, the Fermi level lies closer to the conduction band minimum, whereas in the case of semi-insulating Mg-codoped samples, the Fermi level lies lower within the bandgap, as Mg is known to be a deep acceptor.[20]

In particular, prior to proton irradiation, the TL glow curve consists of at least an intense peak centered at ~380 K, with a broadening at ~430 K (which might indicate the presence of a satellite peak) and two smaller peaks at ~485 and ~540 K. It should be noted that the small increase observed for temperatures above ~600 K is not a TL signal but rather due to the blackbody radiation.

It is possible to observe a few differences in the TL glow curve obtained for the irradiated sample. Note that the registered TL intensity was higher overall, which is likely related to the larger sample area. Considering the first measurement after proton irradiation, the most intense peak is observed to shift toward higher temperatures (~400 K), keeping the shoulder at ~430 K, while the region between ~450 and 600 K is enhanced with respect to the most intense peak. The shape of this region is quite complex, corresponding to the superposition of several peaks. Moreover, the curve obtained during a second measurement, performed consecutively and in the same conditions, shows a global intensity decrease, mostly noticeable in the region between 450 and 600 K, which is likely related with the unintentional annealing of the sample and the removal of some defects during the first measurement, where it was heated to temperatures of about 620 K.

These preliminary results show that there are defect levels induced by the proton irradiation that are able to enhance the Cr^{3+} emission, similar to our previous results on samples without Mg-codoping where proton-induced defects were shown to act as sensitizer enabling the Cr^{3+} emission.[13,14]

2.2. TL after Annealing. In order to assess the removal of defects during annealing, both the pristine and irradiated samples were annealed in situ at 923 K (650 °C) for 10 s under a constant N_2 flow. Afterward, both samples were irradiated with β^- radiation for 400 s before being measured with a heating rate of 2 K/s up to a temperature of 623 K. The glow curves for the two samples are shown in Figure 2, both before and after annealing. It should be noted that the measurements after annealing were performed after all of the measurements presented in Sections 2.3.−2.5., which were performed on unannealed samples.

Upon annealing, the shape and position of the TL glow curves of both the pristine and irradiated samples are very similar (Figure 2); the main difference between the samples lies in the intensity of the curve. This is consistent with the previous discussion regarding the size of the two samples: since the irradiated sample is larger than the pristine one, its TL signal is proportionally larger. Notably, these results show that the irradiation-induced defects can be efficiently removed upon annealing at 923 K. Consequently, this suggests that this material has a potential for utilization as a TL passive dosimeter, with the possibility of reuse after annealing.

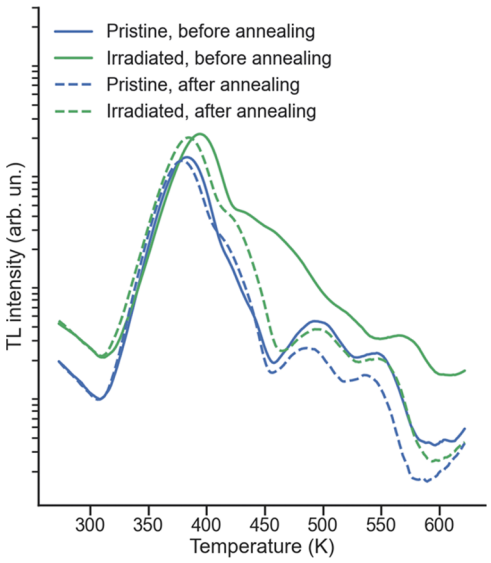

Figure 2. TL glow curves before and after annealing at 923 K, on a logarithmic scale, for both the pristine and irradiated samples.

2.3. Dose-Dependence of TL. In order to assess the kinetic order of the trapping/detrapping processes, the effect of the irradiation dose was investigated by exposing both the pristine and proton-irradiated samples to β^- radiation for 200 s (corresponding to a dose of 14.6 Gy in quartz coarse grains on stainless steel discs) before heating the sample up to 620 K with a heating rate of 2 K/s. When retrapping of electrons can be neglected (first-order kinetics), the maximum of the TL curve is independent of the concentration of trapped charges (i.e., irradiation dose). In contrast, in second-order kinetics, glow peak maxima are expected to shift to higher temperatures for increasing concentration of trapped charges[30,31] since the carrier recombination is delayed by the retrapping.

The glow curves obtained for the 200 s irradiation and for the previous 400 s irradiation (Figure 3) show that most of the observed structures appear at similar temperatures for both irradiation times, which is compatible with first-order kinetics. However, a peak is clearly observed at ~490 K for the higher irradiation dose but not in the low-dose curve. For the proton-irradiated sample, the positions for a higher irradiation dose are slightly shifted toward the high-temperature side, by less than ~10 K, which may be attributed to a temperature shift due to the poor thermal conductivity of β-Ga_2O_3. Moreover, the low-dose curve shows a peak centered at ~545 K (which was already present in the pristine sample) that does not correspond to any visible feature of the high-dose curve, while the latter shows a peak at ~570 K that does not have a clear counterpart in the low-dose curve. It is possible that these two peaks correspond to the same trap, which is not compatible with first-order kinetics and thus the associated

https://doi.org/10.1021/acsomega.3c06429
ACS Omega 2023, 8, 47874−47882

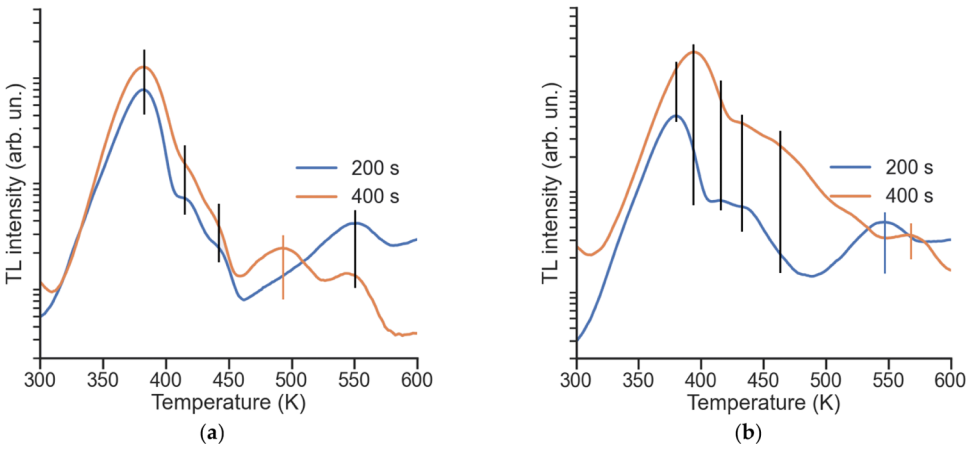

Figure 3. TL glow curves after exposure to β^- radiation for 200 or 400 s, for the pristine (a) and proton-irradiated samples (b), in logarithmic scale. The black bars represent features that are present in both curves, while the colored bars identify features present only on the curve of the corresponding color.

glow peak shifts toward higher temperatures upon higher irradiation doses.

These observations are consistent with a complex glow curve comprising several overlapping glow peaks which conform, to a good approximation, to first-order kinetics, with the possible exception of the peak(s) at temperatures above ~500 K. This result is in agreement with the work by Luchechko et al., where the glow curves were fitted using elementary first-order glow peaks.[15] On the other hand, Islam et al. report nearly symmetrical, broad glow peaks that were well-approximated by Gaussians, which might be indicative of second-order kinetics.[16] In the present case, the glow peaks are also broad, although this can also be explained by the superposition of several elementary glow peaks, by a gradient in the heating rate due to the thickness of the samples (i.e., due to the thickness of the sample and finite thermal conductivity, there is a thermal lag between the heating element temperature and the sample), or even by the inhomogeneity of the β^- irradiation dose with depth (i.e., the deeper regions of the sample are subjected to an effective irradiation dose which is smaller than for the regions closer to the surface).

2.4. T_M-T_{STOP} Method at Low Heating Rate. Considering the previous discussion, the next measurements were performed employing a lower heating rate in order to reduce the thermal lag issues, which can lead to errors in the determination of the activation energy of up to 30%.[32] This problem is worsened by the low thermal conductivity of Ga_2O_3. Hence, the heating rate was reduced to 0.1 K/s. The irradiation was performed for 400 s, and the measurement followed the T_M-T_{STOP} method.[31] In this method, each TL sweep is preceded by a preheating step at a temperature T_{STOP}, while the position T_M of the first maximum of the TL glow curve is monitored. This allows the traps to be gradually depopulated and offers further information about the kinetics order. In the present work, T_{STOP} varies from 328 to 388 K in steps of 5 K (marked by symbols in Figure 4). The TL glow curves and the T_M-T_{STOP} plots (Figure 4) indicate the presence of at least three glow peaks, with positions that remain approximately the same before and after the proton irradiation, suggesting that the traps are similar in both cases. A work by Islam et al.,[16] using a heating rate of 1 K/s, reports the existence of two glow peaks in Mg-doped Ga_2O_3: a very intense peak centered at ~383 K and a less intense peak centered at ~473 K. However, their excitation was performed using UV light at 83 K, which can severely alter the shape of the glow curves.[33] On the other hand, Luchechko et al.[24] used the same heating rate of 0.1 K/s to study Mg-doped Ga_2O_3, with the excitation performed using X-rays at room temperature. The glow curve obtained in the previously mentioned work was deconvoluted on four elementary peaks: two very low intensity peaks centered at 280 and 320 K, a more intense peak centered at 430 K, and two very intense peaks at 354 and 385 K, which are overlapped. The observed glow curve shape was very similar to the results of the present work, although at consistently higher temperatures. In a different work on Cr-, Mg-codoped Ga_2O_3, Luchechko et al. reported six glow peaks (at temperatures of 285, 300, 320, 354, 385, and 430 K), and the dominant peak was the one centered at 320 K, which was correlated with the Cr content.[15] As before, the overall shape of the glow curve is very similar to that in the present work, in spite of the different peak positions.

2.5. TL Glow Curve Fitting. In order to clarify the nature of the involved traps, it is possible to deconvolute the curve by fitting a general-order expression for each glow peak, which is given by[31]

$$I(T) = \frac{n_0 S''}{\beta}\exp\left(-\frac{E}{kT}\right) \times \left[1 - (1-b)\frac{S''}{\beta}\int_{T_0}^{T}\exp\left(-\frac{E}{kT'}\right)dT'\right]^{b/1-b} \quad (1)$$

where S'' is a characteristic frequency, b is the general kinetics order parameter, β is the heating rate, E is the trap activation energy, n_0 is the density of traps at the initial temperature $T = T_0$. Since each glow peak is characterized by a set of four parameters, it is desirable to restrict their range before fitting. In this context, one can use the initial rise method: considering only the initial portion of the curve with intensities below ~10% of the maximum intensity of the glow peak, the activation energy can be estimated from an Arrhenius equation given by[30]

$$\ln I(T) = \ln\frac{n_0 S''}{\beta} - \frac{E}{kT} \quad (2)$$

https://doi.org/10.1021/acsomega.3c06429
ACS Omega 2023, 8, 47874−47882

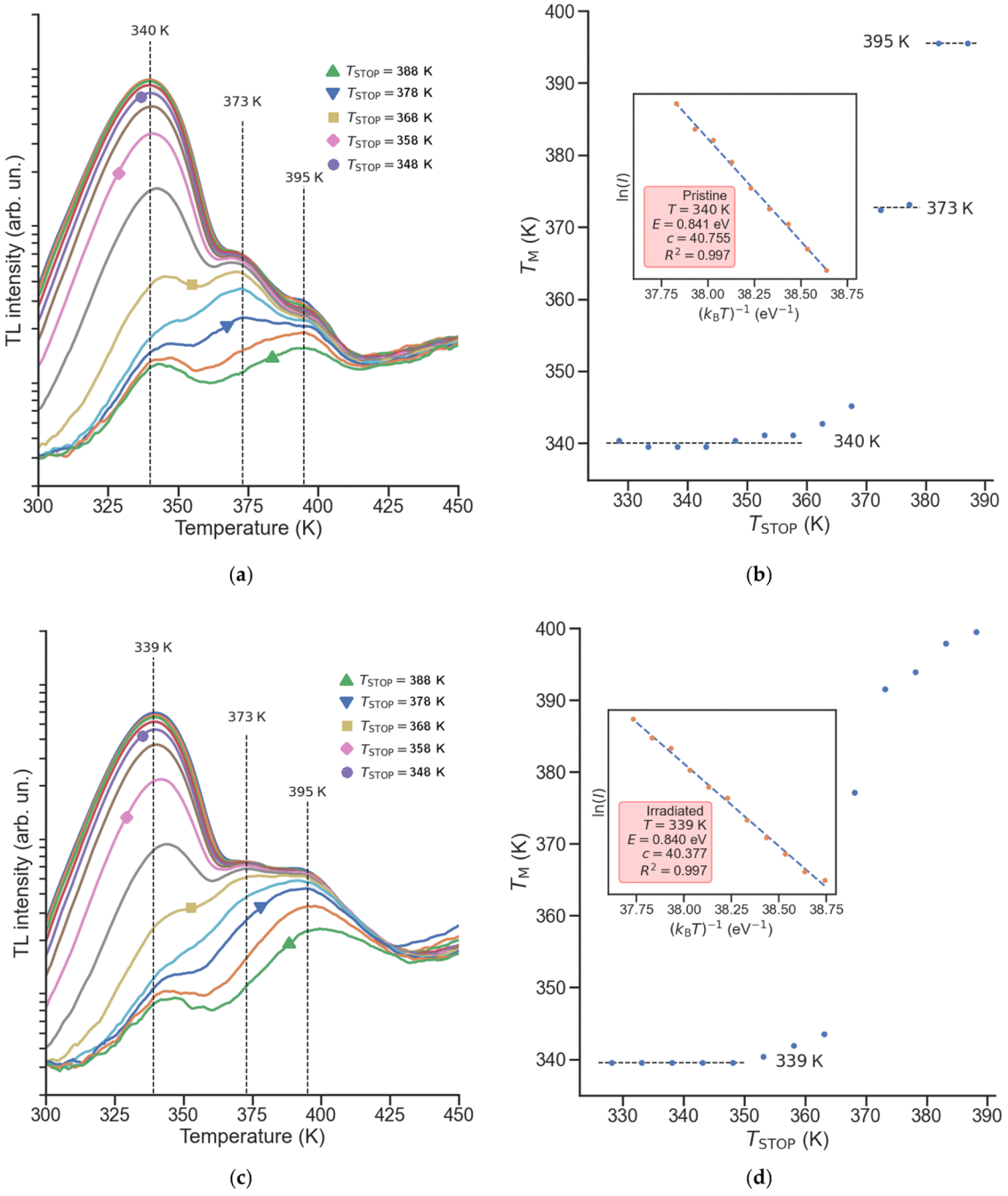

Figure 4. TL glow curves for the pristine sample (a) and the corresponding T_M-T_{STOP} plots (b), as well as the TL glow curves for the ion-irradiated sample (c) and the corresponding T_M-T_{STOP} plots (d). Some values of T_{STOP} were marked with symbols in parts (a) and (c). The dashed lines are guides to mark the flat regions of the plots and the corresponding glow peaks. The insets show the initial rise fits for each of the samples, according to eq 2, with $c = \ln\frac{n_0 s''}{\beta}$.

which is independent of b. However, since it relies on the initial portion of the curve, this method requires the glow peaks to be sufficiently separated. Considering the results of the T_M-T_{STOP} method, the strong overlap among the peaks hinders the application of this method, since the first peak was never fully thermally bleached. Hence, this method was applied to the lowest temperature peak only, yielding activation energies of (0.841 ± 0.017) and (0.840 ± 0.016) eV for the pristine and irradiated samples, respectively. The corresponding fits are shown as insets in Figure 4(b,d), respectively.

These activation energies are similar between both samples, thus suggesting that they correspond to the same type of traps. This also compares well with previous experimental works. In particular, a glow peak centered at 354 K, corresponding to a trap with an activation energy of 0.84 eV, has been reported by Luchechko et al. in Cr-, Mg-codoped Ga_2O_3, which was assigned to 3-fold coordinated oxygen vacancies.[24] Moreover, Gao et al. also reported a level with an activation energy of 0.82 eV,[26] while Lenyk et al. reported a glow peak centered at 349 K, corresponding to an activation energy of 0.84 eV, in Fe-doped Ga_2O_3, which is assigned to the $Fe^{2+/3+}$ level.[21] In this

https://doi.org/10.1021/acsomega.3c06429
ACS Omega 2023, 8, 47874−47882

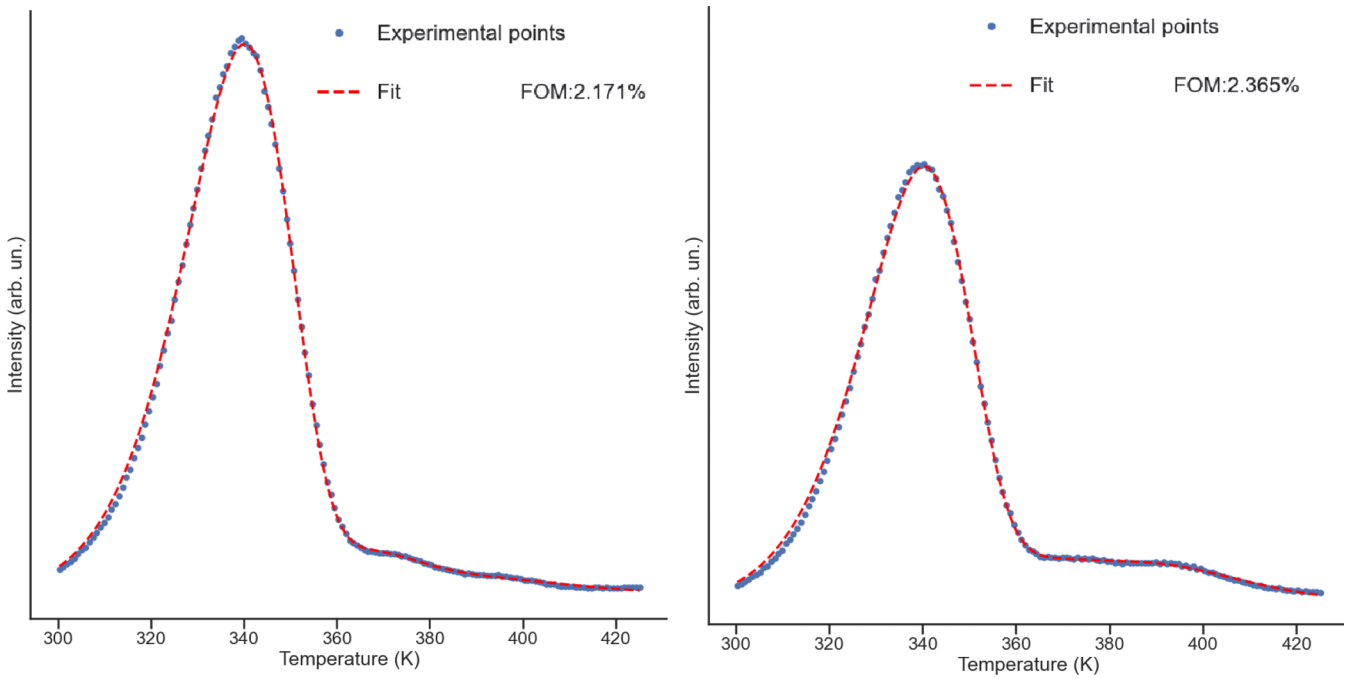

Figure 5. Fitting of the TL glow curves for the pristine (a) and irradiated (b) samples, using three glow peaks given by eq 1. The FOM values were calculated by using eq 3.

context, Ingebrigtsen et al. also calculated two close-by levels: the 3+/2+ level of $Ga_{O(I)}$, with an activation energy of 0.83 eV, and the -/2- level of a $V_{O(II)} - (Ga_i - V_{Ga})$ complex, with an activation energy of 0.84 eV.[22] A compilation of these levels and assignments is given in Table S1 of the Supporting Information.

Since the 339/340 K glow peak was never fully thermally cleaned, the initial rise method is not suitable for the remaining analysis. Hence, considering the results of Subsections 2.4. and 2.5. and following Luchechko et al.,[24] the remaining two peaks at 373 and 395 K in this work were assigned to their elementary peaks at 385 and 430 K, with activation energies of 1.0 and 1.1 eV, respectively. This assumption is reasonable, given that the energy associated with the peaks at 339 and 340 K in this work matches well with the peak at 354 K in the aforementioned work. Under this assumption, the experimental data were fitted to the sum of three general-order kinetics glow curves, according to eq 1, with the activation energies as fixed parameters. The fitting quality is assessed with the usual TL figure of merit (FOM)[30]

$$\mathrm{FOM} = \frac{\sum_T |I_{\mathrm{exp}}(T) - I_{\mathrm{fit}}(T)|}{\sum_T I_{\mathrm{fit}}(T)} \quad (3)$$

where $I_{\mathrm{exp}}(T)$ and $I_{\mathrm{fit}}(T)$ are the TL intensities at temperature T obtained experimentally and via the fit, respectively. Figure 5 shows the experimental data and fits; the corresponding parameters are listed in Table 1.

The obtained fits have a FOM below 2.5%, thus indicating a generally good agreement between the employed model and the experimental data. The main differences between the fits and the experimental data occur in the low-temperature portion of the first peak, which can be explained by the fact that the peak actually results from the overlap of multiple peaks. Hence, both the intensity and the order of this peak may be slightly underestimated. On the other hand, the kinetic parameters for this peak are very consistent between the pristine and the irradiated sample, while the kinetic order is indeed compatible with first order, as expected from the dose study. Moreover, they are in good agreement with the energy and frequency reported by Lenyk et al. (0.84 eV and 9.5×10^{10} Hz, respectively), although the kinetic order estimated by these authors is somewhat larger (1.87).

A similar consistency between the two samples is also observed for the other two peaks, with the exception of the kinetic order parameter. Since this parameter controls the symmetry between the high- and low-temperature sides of the glow peak, the observed differences may result from some compensation between these values that yield similar profiles in the fitting: the low-temperature side of the peak at 395 K can be increased at the expense of the decrease of the high-temperature side of the peak at 373 K, and vice versa. On the

Table 1. Fitting Parameters of the Glow Curves of the Pristine and Irradiated Samples, as shown in Figure 4

peak temperature	parameter	pristine	irradiated
339/340 K	S'' (Hz)	2.401×10^{10}	2.519×10^{10}
	n_0 (arb. un.)	2.230×10^{6}	1.664×10^{6}
	b (−)	1.001	1.000
	E (eV)	0.840	0.841
373 K	S'' (Hz)	5.726×10^{11}	8.345×10^{11}
	n_0 (arb. un.)	2.028×10^{5}	3.340×10^{5}
	b (−)	1.420	3.186
	E (eV)	1.000	1.000
395 K	S'' (Hz)	9.270×10^{11}	9.639×10^{11}
	n_0 (arb. un.)	1.318×10^{5}	1.467×10^{5}
	b (−)	2.726	2.008
	E (eV)	1.100	1.100
FOM		2.171%	2.365%

https://doi.org/10.1021/acsomega.3c06429
ACS Omega 2023, 8, 47874−47882

other hand, the observed values of the frequency parameter have reasonable orders of magnitude, lying between 10^{10} and 10^{12} Hz, which are consistent with the Debye frequency of the order of 10^{13} Hz for Ga_2O_3 (Debye temperature of 723 K).[34] Overall, the consistency of the parameters between the pristine and irradiated samples suggests that the traps correspond to native defects, whose concentration is increased by the proton irradiation.

Following Luchechko et al., the peak at 373 K may then be assigned to O(III) vacancies, with a 4-fold coordination.[24] However, in a subsequent study, Luchechko et al. assigned the O(III) vacancies to a trap with an activation energy 0.94 eV instead, which shows that these ascriptions are not trivial. In this context, Zhang et al. also report a trap E3 with an activation energy of 1.00 eV by DLTS, although no tentative assignment is suggested.[25] Moreover, they show that its concentration is ten times lower than another one with an activation energy of 0.82 eV, which is also approximately the same ratio as the traps at 1.0 and 0.84 eV described in the present work. Moreover, Ingebrigtsen et al. have also observed a trap with activation energy 1.01 eV by DLTS in unintentionally doped pristine and proton-irradiated samples, having assigned it to E3 as well.[22]

Lastly, both works by Luchechko et al. report the presence of a trap at 1.1 eV, but no definite assignment is given. Two possible assignments for the peak at 395 K are the 2+/+ level of Ga_i, with an activation energy of 1.12 eV, or the 2+/+ level of $Ga_{O(II)}$, with an activation energy of 1.11 eV, by comparison with the theoretical calculations by Ingebrigtsen et al.[22] For an overview of the already-reported defect levels and the different crystallographic sites in the lattice, refer to the Supporting Information.

3. CONCLUSIONS

In conclusion, this work presents a detailed TL analysis of Cr-, Mg-codoped Ga_2O_3 samples before and after proton irradiation. These samples have a strong TL signal at the Cr^{3+} wavelengths, even prior to being irradiated with protons.

Upon proton irradiation, the TL signal is enhanced due to the introduction of defect levels that trap electrons. A detailed TL study, which included employing different radiation doses, a thorough T_M-T_{STOP} measurement, and a computational glow curve fitting routine using three elementary glow peaks, allowed the determination of the kinetic parameters for each of them. Based on their activation energies, it was possible to assign each of these traps to different intrinsic and extrinsic defects by comparing with literature data. These include a 0.84 eV level corresponding to 3-fold-coordinated oxygen vacancies or the 2+/3+ charge transfer level of Fe contaminants[21,24] and a 1.0 eV level associated with 4-fold-coordinated oxygen vacancies.[24] A 1.1 eV level was also identified, which is consistent with previous observations, although no definitive assignment is given. Upon comparison with theoretical predictions, it is possible to tentatively assign it to the 2+/+ level of gallium interstitials (1.12 eV) or the 2+/+ level of gallium−oxygen(I) antisites (1.11 eV).[22]

Finally, it was shown that the pristine glow curves can be recovered by annealing at 923 K, allowing the defects induced during proton irradiation to be removed. Hence, this work further contributes to the understanding of the trapping and recombination dynamics of electrons and holes in Ga_2O_3.

4. MATERIALS AND METHODS

In this study, a high-quality single-crystal Cr-doped β-Ga_2O_3 sample with a (100) surface orientation was grown by a modified edge-defined film-fed growth (EFG) method at the State Key Laboratory of Crystal Materials.[28] The growth method is described in detail elsewhere,[28] as well as ion-beam-induced luminescence, photoluminescence, X-ray diffraction, and Raman spectroscopy results.[13,14] The samples employed in this work have a thickness of about 500 μm and were obtained by cleaving the crystal into two samples with lateral dimensions of a few mm. The PIXE maps in the Supporting Information show the homogeneous distribution of the Cr (0.028 atom %) dopant and Fe (0.008 atom %) contaminant.

The proton irradiation was performed at the 2.5 MV Van de Graaff accelerator at the Laboratory of Accelerators and Radiation Technologies of Instituto Superior Técnico, University of Lisbon,[13,35] with a circular beam with a ∼ 3 mm radius, which was scanned along the length of the sample. Three different irradiation energies were employed: 1000, 1500, and 2000 keV. For each energy, the sample was irradiated up to a fluence of 10^{15} protons/cm^2. The nominal beam current was ∼5 nA. The SRIM simulations of the vacancy profiles for these irradiation conditions are shown in the Supporting Information.

The thermoluminescence measurements were performed using a Risø Thermoluminescence/Optically stimulated luminescence reader (TL/OSL-DA-20) manufactured by DTU Physics, at the Luminescence Dating Laboratory of Instituto Superior Técnico, University of Lisbon. The excitation was performed using a $^{90}Sr/^{90}Y$ β^- source (with a nominal activity of 40 mCi and a dose rate in quartz coarse grains on stainless steel discs of 0.073 ± 0.002 Gy/s). A commercial detection filter RG630 was employed in order to monitor the spectral region with wavelengths above ∼630 nm. The penetration depth of electrons from this decay (with energies of 193 and 933 keV) is ∼50 μm and ∼500 μm, respectively, as estimated using the PENELOPE code.[36]

■ ASSOCIATED CONTENT

Supporting Information

The Supporting Information is available free of charge at https://pubs.acs.org/doi/10.1021/acsomega.3c06429.

Additional details, including SRIM simulations and PIXE maps and spectra, as well as a table summarizing literature results (PDF)

■ AUTHOR INFORMATION

Corresponding Author

Duarte Magalhães Esteves − *INESC MN, Lisboa 1000-029, Portugal; IPFN, Instituto Superior Técnico, University of Lisbon, Lisboa 1049-001, Portugal;* orcid.org/0000-0001-8566-9245; Email: duarte.esteves@tecnico.ulisboa.pt

Authors

Ana Luísa Rodrigues − *C^{2}TN, Instituto Superior Técnico, University of Lisbon, Bobadela 2695-066, Portugal; DECN, Instituto Superior Técnico, University of Lisbon, Bobadela 2695-066, Portugal*

Maria Isabel Dias − *C^{2}TN, Instituto Superior Técnico, University of Lisbon, Bobadela 2695-066, Portugal; DECN,*

https://doi.org/10.1021/acsomega.3c06429
ACS Omega 2023, 8, 47874−47882

Instituto Superior Técnico, University of Lisbon, Bobadela 2695-066, Portugal

Luís Cerqueira Alves − *C^2TN, Instituto Superior Técnico, University of Lisbon, Bobadela 2695-066, Portugal; DECN, Instituto Superior Técnico, University of Lisbon, Bobadela 2695-066, Portugal*

Zhitai Jia − *State Key Laboratory of Crystal Materials, Shandong University, Jinan 250100, China;* orcid.org/0000-0002-7534-8082

Wenxiang Mu − *State Key Laboratory of Crystal Materials, Shandong University, Jinan 250100, China*

Katharina Lorenz − *INESC MN, Lisboa 1000-029, Portugal; IPFN, Instituto Superior Técnico, University of Lisbon, Lisboa 1049-001, Portugal; DECN, Instituto Superior Técnico, University of Lisbon, Bobadela 2695-066, Portugal*

Marco Peres − *INESC MN, Lisboa 1000-029, Portugal; IPFN, Instituto Superior Técnico, University of Lisbon, Lisboa 1049-001, Portugal; DECN, Instituto Superior Técnico, University of Lisbon, Bobadela 2695-066, Portugal*

Complete contact information is available at: https://pubs.acs.org/10.1021/acsomega.3c06429

Author Contributions

D.M.E., K.L., and M.P. contributed in conceptualization; D.M.E. and A.L.R. contributed in methodology; D.M.E. contributed in software; M.I.D., Z.J., K.L., and M.P. contributed in validation; D.M.E. contributed in formal analysis; D.M.E., A.L.R., L.C.A., and W.M. contributed in investigation; M.I.D., L.C.A., Z.J., K.L., and M.P. contributed in resources; D.M.E., A.L.R., and L.C.A. contributed in data curation; D.M.E. contributed in writing—original draft preparation; A.L.R., M.I.D., L.C.A., W.M., Z.J., K.L., and M.P. contributed in writing—review and editing; D.M.E. contributed in visualization; K.L. and M.P. contributed in supervision; K.L. and M.P. contributed in project administration; M.I.D. and K.L. contributed in funding acquisition. All authors have given approval to the final version of the manuscript.

Notes

The authors declare no competing financial interest.

■ ACKNOWLEDGMENTS

INESC MN acknowledges Fundação para a Ciência e a Tecnologia (FCT) for funding the Research Unit INESC MN (UID/05367/2020) through Plurianual BASE and PROGRAMATICO financing. This work has also received funding from the National funds through FCT under the program grants 2022.05329.PTDC, PTDC/CTM-CTM/3553/2020, UIDB/04349/2020, UID/Multi/04349/2020, and 2022.09585.BD, as well as the EU H2020 Project No. 824096 "RADIATE".

■ ABBREVIATIONS

DLTS, deep-level transient spectroscopy
DLOS, deep-level optical spectroscopy
EFG, edge-defined film-fed growth
FOM, figure of merit
IBIL, ion-beam-induced luminescence
IR, infrared
PIXE, particle-induced X-ray emission
RT, room temperature
SRIM, stopping and ranges of ions in matter
TL, thermoluminescence
UV, ultraviolet

■ REFERENCES

(1) Stepanov, S. I.; Nikolaev, V. I.; Bougrov, V. E.; Romanov, A. E. Gallium Oxide: Properties and Applications − a Review. *Rev. Adv. Mater. Sci.* **2016**, *4*, 63−86.

(2) Pearton, S. J.; Yang, J.; Cary, P. H.; Ren, F.; Kim, J.; Tadjer, M. J.; Mastro, M. A. A Review of Ga_2O_3 Materials, Processing, and Devices. *Appl. Phys. Rev.* **2018**, *5* (1), No. 011301.

(3) *Gallium Oxide: Materials Properties, Crystal Growth, and Devices*; Higashiwaki, M.; Fujita, S., Eds.; Springer International Publishing, 2020. DOI: 10.1007/978-3-030-37153-1.

(4) Orita, M.; Ohta, H.; Hirano, M.; Hosono, H. Deep-Ultraviolet Transparent Conductive β-Ga_2O_3 Thin Films. *Appl. Phys. Lett.* **2000**, *77* (25), 4166−4168.

(5) Chikoidze, E.; Fellous, A.; Perez-Tomas, A.; Sauthier, G.; Tchelidze, T.; Ton-That, C.; Huynh, T. T.; Phillips, M.; Russell, S.; Jennings, M.; Berini, B.; Jomard, F.; Dumont, Y. P-Type β-Gallium Oxide: A New Perspective for Power and Optoelectronic Devices. *Mater. Today Phys.* **2017**, *3*, No. 118.

(6) Xu, J.; Zheng, W.; Huang, F. Gallium Oxide Solar-Blind Ultraviolet Photodetectors: A Review. *J. Mater. Chem. C* **2019**, *7* (29), 8753−8770.

(7) Almaev, A. V.; Chernikov, E. V.; Davletkildeev, N. A.; Sokolov, D. V. Oxygen Sensors Based on Gallium Oxide Thin Films with Addition of Chromium. *Superlattices Microstruct.* **2020**, *139*, No. 106392.

(8) Hemmer, E.; Benayas, A.; Légaré, F.; Vetrone, F. Exploiting the Biological Windows: Current Perspectives on Fluorescent Bioprobes Emitting above 1000 nm. *Nanoscale Horiz.* **2016**, *1* (3), 168−184.

(9) Tippins, H. H. Optical and Microwave Properties of Trivalent Chromium in β-Ga_2O_3. *Phys. Rev.* **1965**, *137* (3A), A865−A871.

(10) Harwig, T.; Kellendonk, F. Some Observations on the Photoluminescence of Doped β-Galliumsesquioxide. *J. Solid State Chem.* **1978**, *24*, No. 255.

(11) Alonso-Orts, M.; et al. Modal Analysis of β-Ga_2O_3:Cr Widely Tunable Luminescent Optical Microcavities. *Phys. Rev. Appl.* **2018**, *9*, No. 64004.

(12) Mykhaylyk, V.; Kraus, H.; Zhydachevskyy, Y.; Tsiumra, V.; Luchechko, A.; Wagner, A.; Suchocki, A. Multimodal Non-Contact Luminescence Thermometry with Cr-Doped Oxides. *Sensors* **2020**, *20*, No. 5259.

(13) Peres, M.; Esteves, D. M.; Teixeira, B. M. S.; Zanoni, J.; Alves, L. C.; Alves, E.; Santos, L. F.; Biquard, X.; Jia, Z.; Mu, W.; Rodrigues, J.; Sobolev, N. A.; Correia, M. R.; Monteiro, T.; Ben Sedrine, N.; Lorenz, K. Enhancing the Luminescence Yield of Cr^{3+} in β-Ga_2O_3 by Proton Irradiation. *Appl. Phys. Lett.* **2022**, *120*, No. 261904.

(14) Esteves, D. M.; Rodrigues, A. L.; Alves, L. C.; Alves, E.; Dias, M. I.; Jia, Z.; Mu, W.; Lorenz, K.; Peres, M. Probing the Cr^{3+} Luminescence Sensitization in β-Ga_2O_3 with Ion-Beam-Induced Luminescence and Thermoluminescence. *Sci. Rep.* **2023**, *13* (1), No. 4882.

(15) Luchechko, A.; Vasyltsiv, V.; Kostyk, L.; Tsvetkova, O.; Pavlyk, B. The Effect of Cr^{3+} and Mg^{2+} Impurities on Thermoluminescence and Deep Traps in β-Ga_2O_3 Crystals. *ECS J. Solid State Sci. Technol.* **2020**, *9*, No. 045008.

(16) Islam, M. M.; Rana, D.; Hernandez, A.; Haseman, M.; Selim, F. A. Study of Trap Levels in β-Ga_2O_3 by Thermoluminescence Spectroscopy. *J. Appl. Phys.* **2019**, *125* (5), No. 055701.

(17) Sun, R.; Ooi, Y. K.; Dickens, P. T.; Lynn, K. G.; Scarpulla, M. A. On the Origin of Red Luminescence from Iron-Doped β-Ga_2O_3 Bulk Crystals. *Appl. Phys. Lett.* **2020**, *117* (5), No. 052101.

(18) Vasyltsiv, V.; Luchechko, A.; Zhydachevskyy, Y.; Kostyk, L.; Lys, R.; Slobodzyan, D.; Jakieła, R.; Pavlyk, B.; Suchocki, A. Correlation between Electrical Conductivity and Luminescence Properties in β-Ga_2O_3:Cr^{3+} and β-Ga_2O_3:Cr,Mg Single Crystals. *J. Vac Sci. Technol. A* **2021**, *39*, No. 033201.

(19) Dang, T.-. H.; Konczykowski, M.; Jaffrès, H.; Safarov, V. I.; Drouhin, H.-. J. Modification of β-Gallium Oxide Electronic

Properties by Irradiation with High-Energy Electrons. *J. Vac Sci. Technol. A* **2022**, *40*, No. 033416.
(20) Neal, A. T.; Mou, S.; Rafique, S.; Zhao, H.; Ahmadi, E.; Speck, J. S.; Stevens, K. T.; Blevins, J. D.; Thomson, D. B.; Moser, N.; Chabak, K. D.; Jessen, G. H. Donors and Deep Acceptors in β-Ga_2O_3. *Appl. Phys. Lett.* **2018**, *113* (6), No. 062101.
(21) Lenyk, C. A.; Gustafson, T. D.; Halliburton, L. E.; Giles, N. C. Deep Donors and Acceptors in β-Ga_2O_3 Crystals: Determination of the $Fe^{2+/3+}$ Level by a Noncontact Method. *J. Appl. Phys.* **2019**, *126* (24), No. 245701.
(22) Ingebrigtsen, M. E.; Kuznetsov, A. Yu.; Svensson, B. G.; Alfieri, G.; Mihaila, A.; Badstübner, U.; Perron, A.; Vines, L.; Varley, J. B. Impact of Proton Irradiation on Conductivity and Deep Level Defects in β-Ga_2O_3. *APL Mater.* **2019**, *7* (2), No. 022510.
(23) Ingebrigtsen, M. E.; Varley, J. B.; Kuznetsov, A. Yu.; Svensson, B. G.; Alfieri, G.; Mihaila, A.; Badstübner, U.; Vines, L. Iron and Intrinsic Deep Level States in Ga_2O_3. *Appl. Phys. Lett.* **2018**, *112* (4), No. 042104.
(24) Luchechko, A.; Vasyltsiv, V.; Kostyk, L.; Tsvetkova, O.; Popov, A. I. Shallow and Deep Trap Levels in X-Ray Irradiated β-Ga_2O_3. *Nucl. Instrum. Methods Phys. Res., Sect. B* **2019**, *441*, 12−17.
(25) Zhang, Z.; Farzana, E.; Arehart, A. R.; Ringel, S. A. Deep Level Defects throughout the Bandgap of (010) β-Ga_2O_3 Detected by Optically and Thermally Stimulated Defect Spectroscopy. *Appl. Phys. Lett.* **2016**, *108*, No. 052105.
(26) Gao, H.; Muralidharan, S.; Pronin, N.; Karim, M. R.; White, S. M.; Asel, T.; Foster, G.; Krishnamoorthy, S.; Rajan, S.; Cao, L. R.; Higashiwaki, M.; Wenckstern, H.; Grundmann, M.; Zhao, H.; Look, D. C.; Brillson, L. J. Optical Signatures of Deep Level Defects in Ga_2O_3. *Appl. Phys. Lett.* **2018**, *112*, No. 242102.
(27) Farzana, E.; Chaiken, M. F.; Blue, T. E.; Arehart, A. R.; Ringel, S. A. Impact of Deep Level Defects Induced by High Energy Neutron Radiation in β-Ga_2O_3. *APL Mater.* **2019**, *7*, No. 022502.
(28) Mu, W.; Jia, Z.; Yin, Y.; Fu, B.; Zhang, J.; Zhang, J.; Tao, X. Solid−Liquid Interface Optimization and Properties of Ultra-Wide Bandgap β-Ga_2O_3 Grown by Czochralski and EFG Methods. *CrystEngComm* **2019**, *21* (17), 2762−2767.
(29) Ziegler, J. F.; Biersack, J. P.; Littmark, U. *SRIM: The Stopping and Range of Ions in Solids*; Pergamon, 1985.
(30) McKeever, S. W. S. *Thermoluminescence of Solids*; Cambridge University Press, 1985. DOI: 10.1017/CBO9780511564994.
(31) McKeever, S. W. S. On the Analysis of Complex Thermoluminescence. Glow-Curves: Resolution into Individual Peaks. *Phys. Status Solidi* **1980**, *62*, 331−340.
(32) Ege, A.; Wang, Y.; Townsend, P. D. Systematic Errors in Thermoluminescence. *Nucl. Instrum. Methods Phys. Res., Sect. A* **2007**, *576* (2), 411−416.
(33) Lu, J. K.; Tung, C. J.; Hsu, P. C. Thermoluminescence Response as a Function of Irradiation Temperature. *Radiat. Eff.* **1983**, *76* (6), 215−219.
(34) Guo, Z.; Verma, A.; Wu, X.; Sun, F.; Hickman, A.; Masui, T.; Kuramata, A.; Higashiwaki, M.; Jena, D.; Luo, T. Anisotropic Thermal Conductivity in Single Crystal β-Gallium Oxide. *Appl. Phys. Lett.* **2015**, *106* (11), No. 111909.
(35) Alves, E.; Lorenz, K.; Catarino, N.; Peres, M.; Dias, M.; Mateus, R.; Alves, L. C.; Corregidor, V.; Barradas, N. P.; Fonseca, M.; Cruz, J.; Jesus, A. An Insider View of the Portuguese Ion Beam Laboratory. *Eur. Phys. J. Plus* **2021**, *136*, No. 684.
(36) OECD. *PENELOPE 2018: A Code System for Monte Carlo Simulation of Electron and Photon Transport*, Workshop Proceedings, Barcelona, Spain, 28 January − 1 February 2019; Organisation for Economic Co-operation and Development: Paris, 2019.

https://doi.org/10.1021/acsomega.3c06429
ACS Omega 2023, 8, 47874−47882